



AMS
American Meteorological Society

Supplemental Material

[© Copyright 2020 American Meteorological Society](#)

Permission to use figures, tables, and brief excerpts from this work in scientific and educational works is hereby granted provided that the source is acknowledged. Any use of material in this work that is determined to be “fair use” under Section 107 of the U.S. Copyright Act or that satisfies the conditions specified in Section 108 of the U.S. Copyright Act (17 USC §108) does not require the AMS’s permission. Republication, systematic reproduction, posting in electronic form, such as on a website or in a searchable database, or other uses of this material, except as exempted by the above statement, requires written permission or a license from the AMS. All AMS journals and monograph publications are registered with the Copyright Clearance Center (<http://www.copyright.com>). Questions about permission to use materials for which AMS holds the copyright can also be directed to permissions@ametsoc.org. Additional details are provided in the AMS Copyright Policy statement, available on the AMS website (<http://www.ametsoc.org/CopyrightInformation>).

Supporting Information for “Response of Vertical Velocities in Extratropical Precipitation Extremes to Climate Change”

Ziwei Li *, Paul O’Gorman

Department of Earth, Atmospheric and Planetary Sciences, Massachusetts Institute of Technology, Cambridge, MA, USA

*ziweili@mit.edu

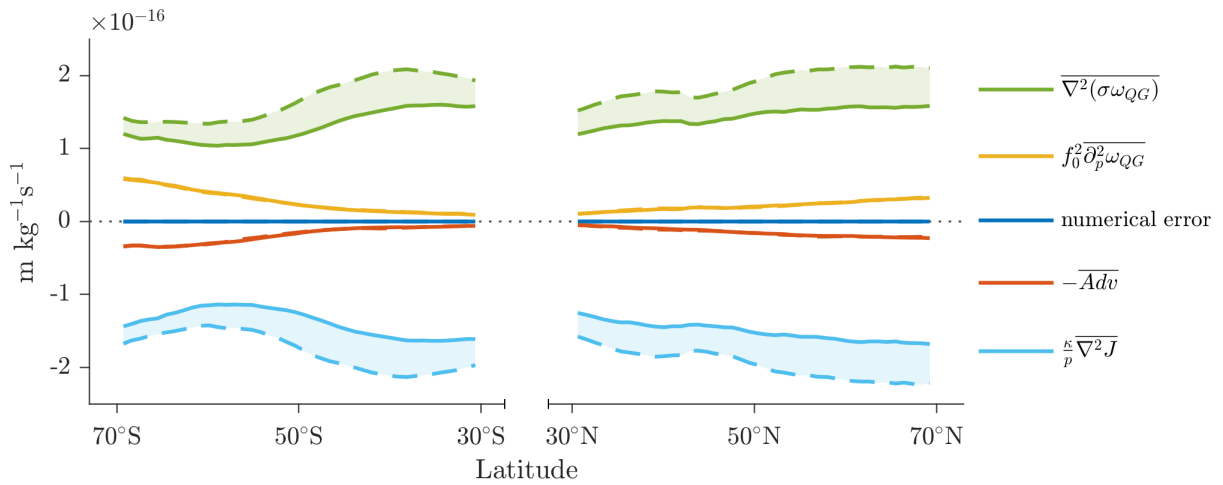


Figure S1. Event- and zonal-mean of terms in the QG- ω equation (Eq. 1) at 500hPa for extratropical precipitation extremes in CESM-LE. Solid lines indicate historical, dashed lines indicate RCP8.5, and shading indicates the response to climate change. Terms on the right-hand side of the equation are shown with a minus sign so that the sum is zero. The darker blue line gives the error in the numerical solution of the QG- ω equation.

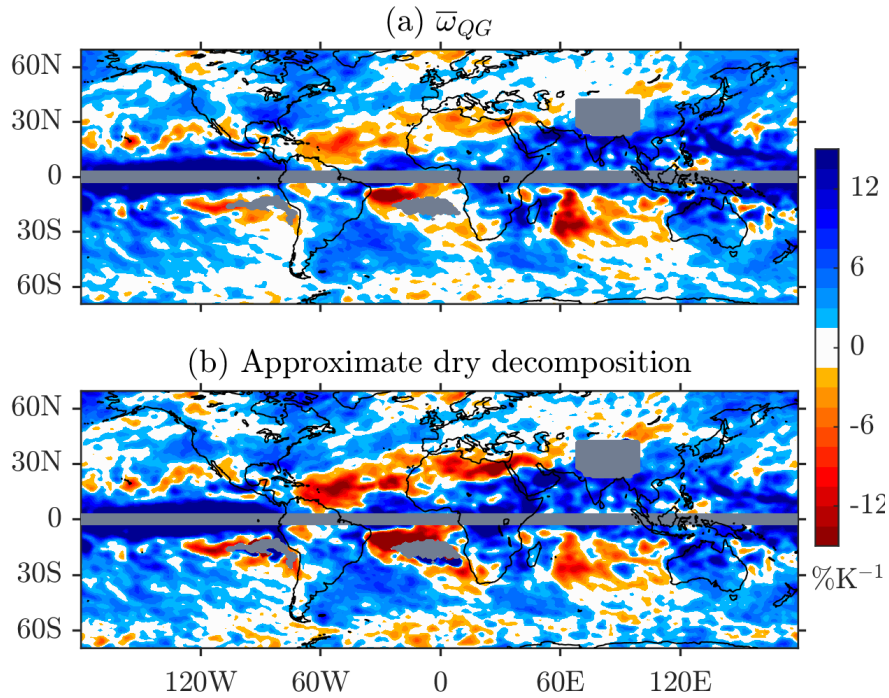


Figure S2. Changes in $\bar{\omega}_{QG}$ (a) from the numerical inversions of the QG- ω equation and (b) as estimated from the approximate dry decomposition (Eq. 7) for vertical velocities at 500hPa associated with precipitation extremes in CESM-LE. Results are expressed as percentage changes relative to the historical climate and normalized by the increase in global-mean surface temperature. Masking and smoothing are as in Fig. 2.

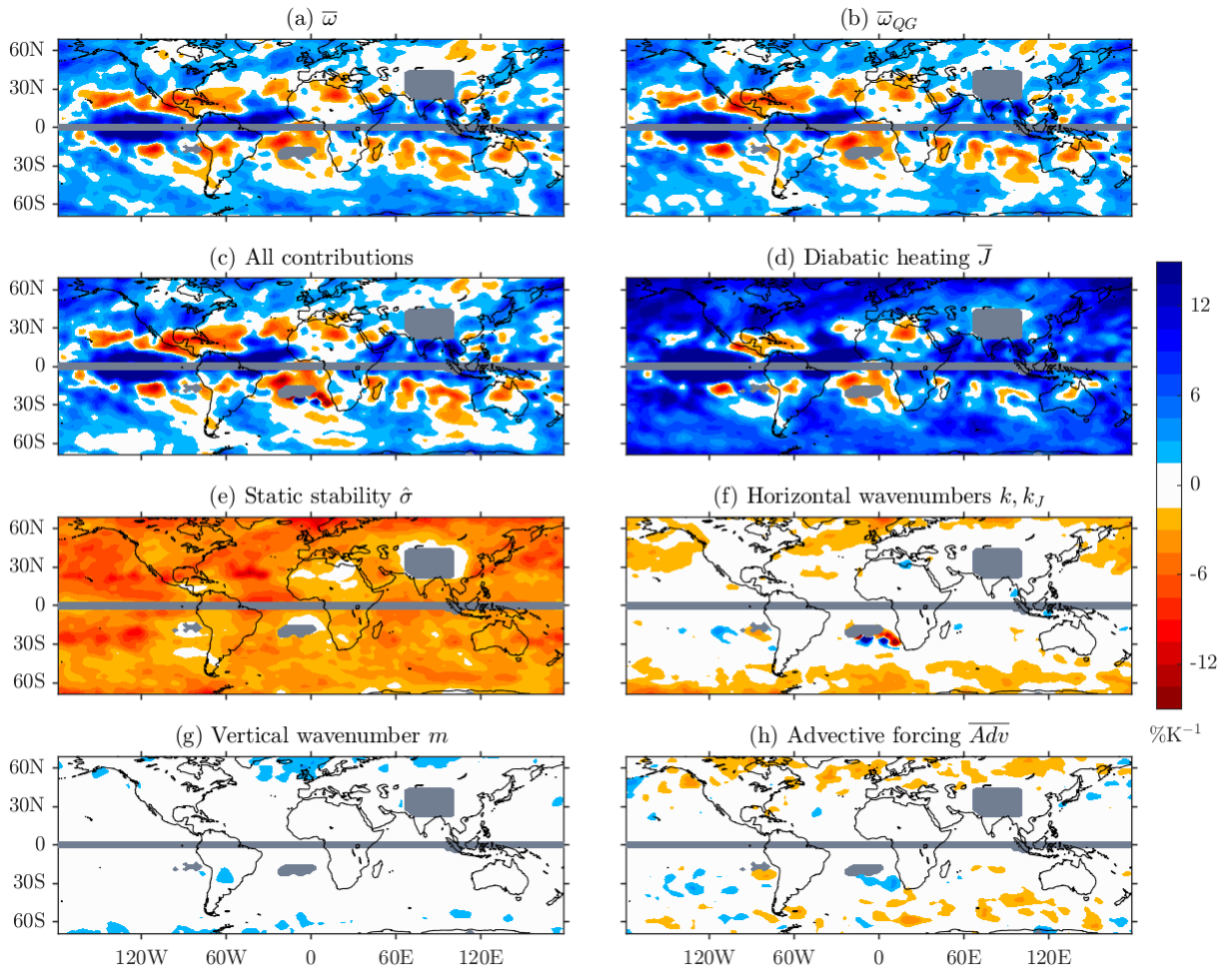


Figure S3. As in Fig. 4, but for 6-hourly events with GFDL-CM3. Grid points with fewer than 15 events are masked.

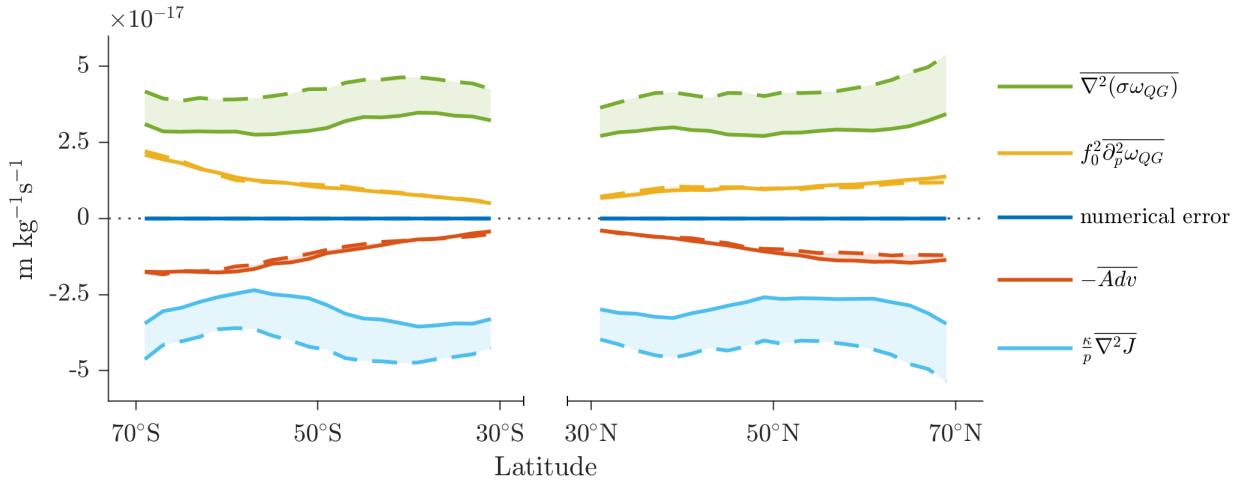


Figure S4. As in Fig. S1, but for GFDL-CM3. (Note the change of scale of the vertical axis)

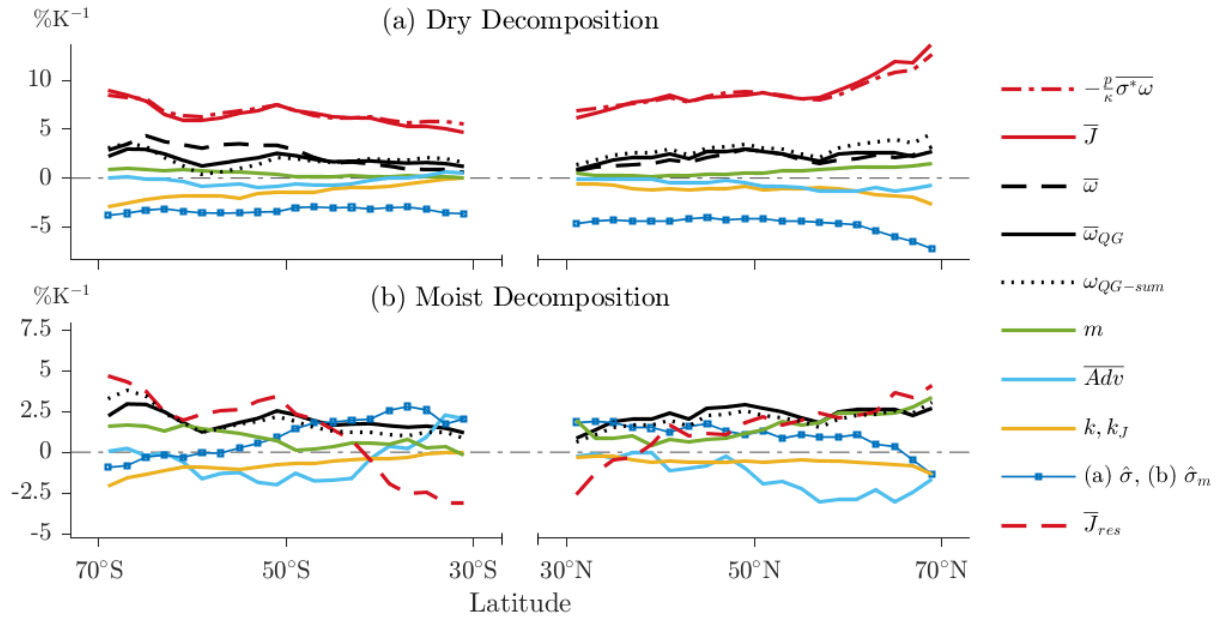


Figure S5. As in Fig. 5, but for GFDL-CM3. (Note the change of scale of the vertical axis)

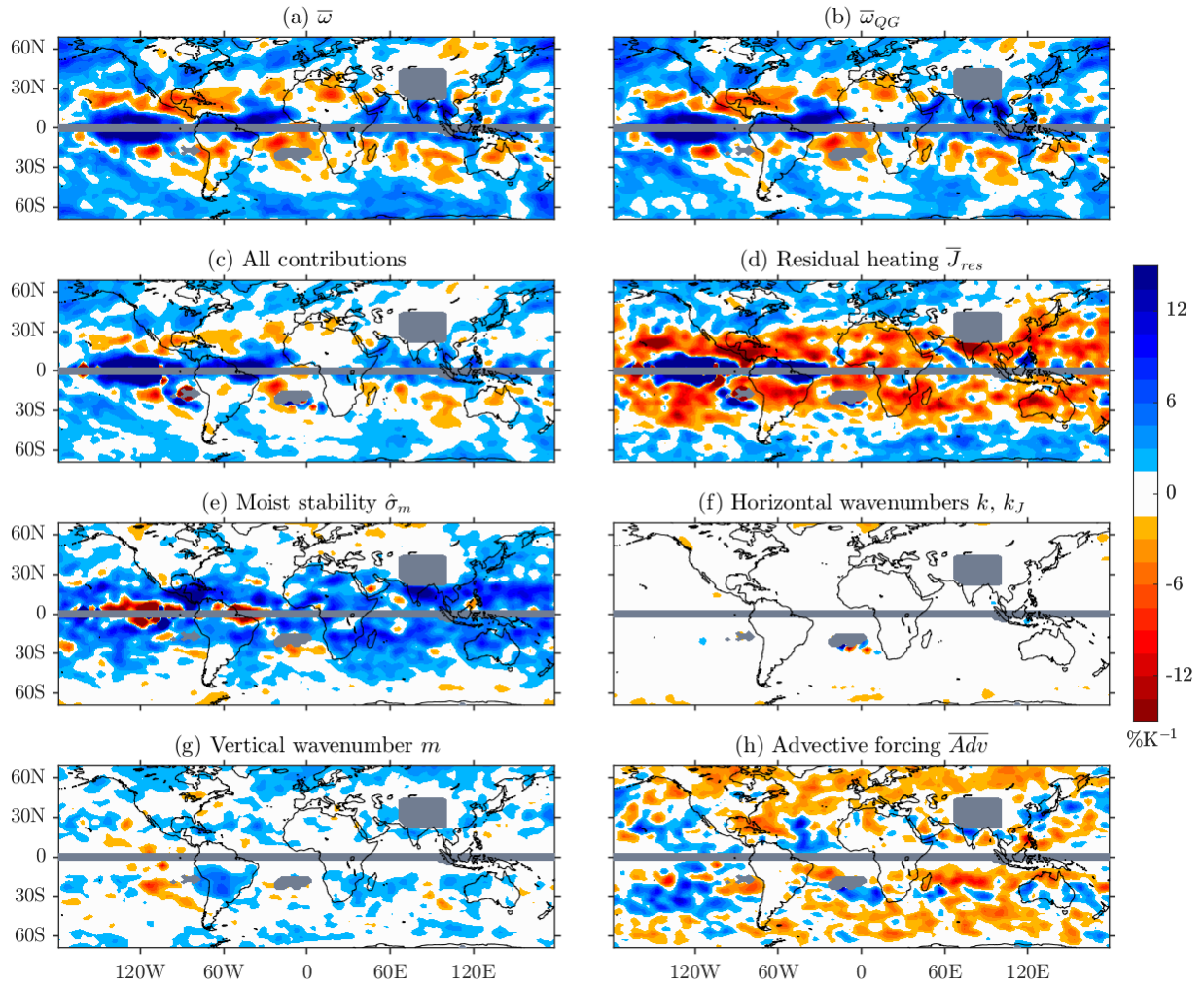


Figure S6. As in Fig. 8, but for GFDL-CM3.

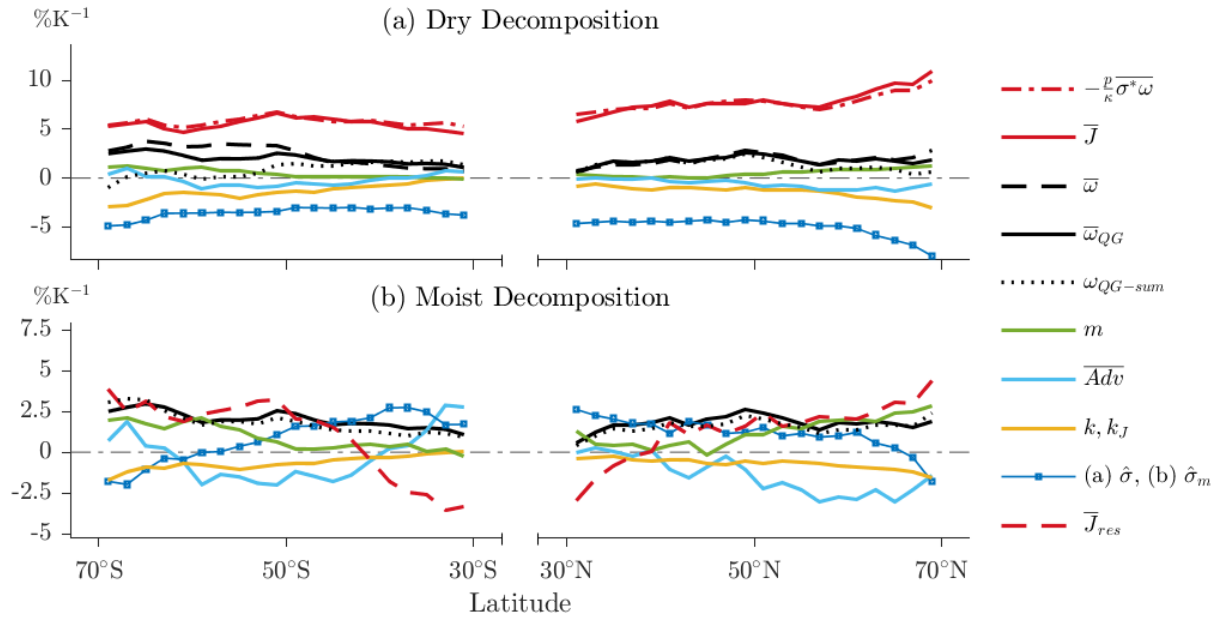


Figure S7. As in Fig. 5, but for GFDL-CM3 and the QG- ω equation is solved using ω taken from the GCM simulations for the lateral- and lower-boundary conditions.

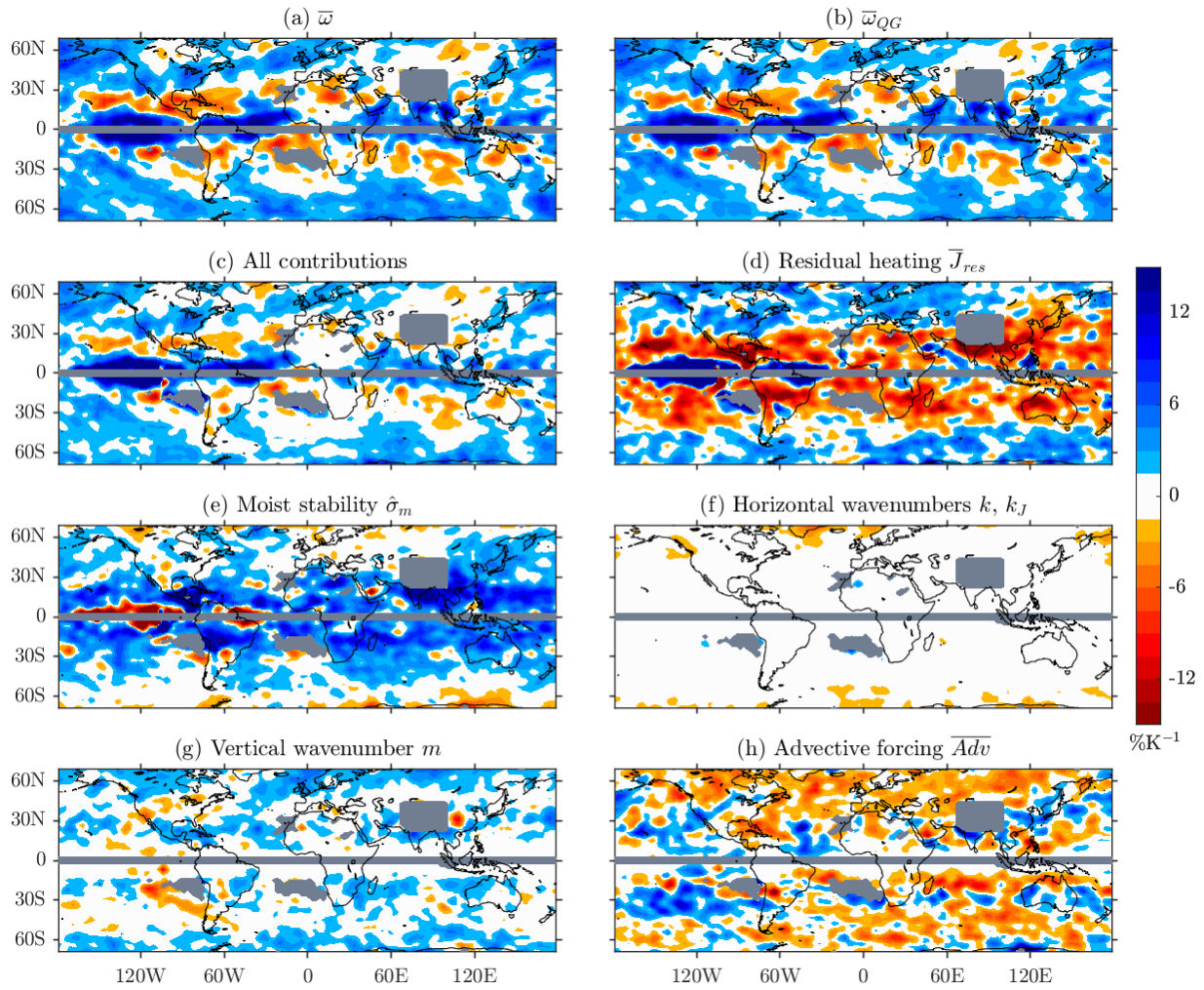


Figure S8. As in Fig. 8, but for GFDL-CM3 and the QG- ω equation is solved using ω taken from the GCM simulations for the lateral- and lower-boundary conditions.

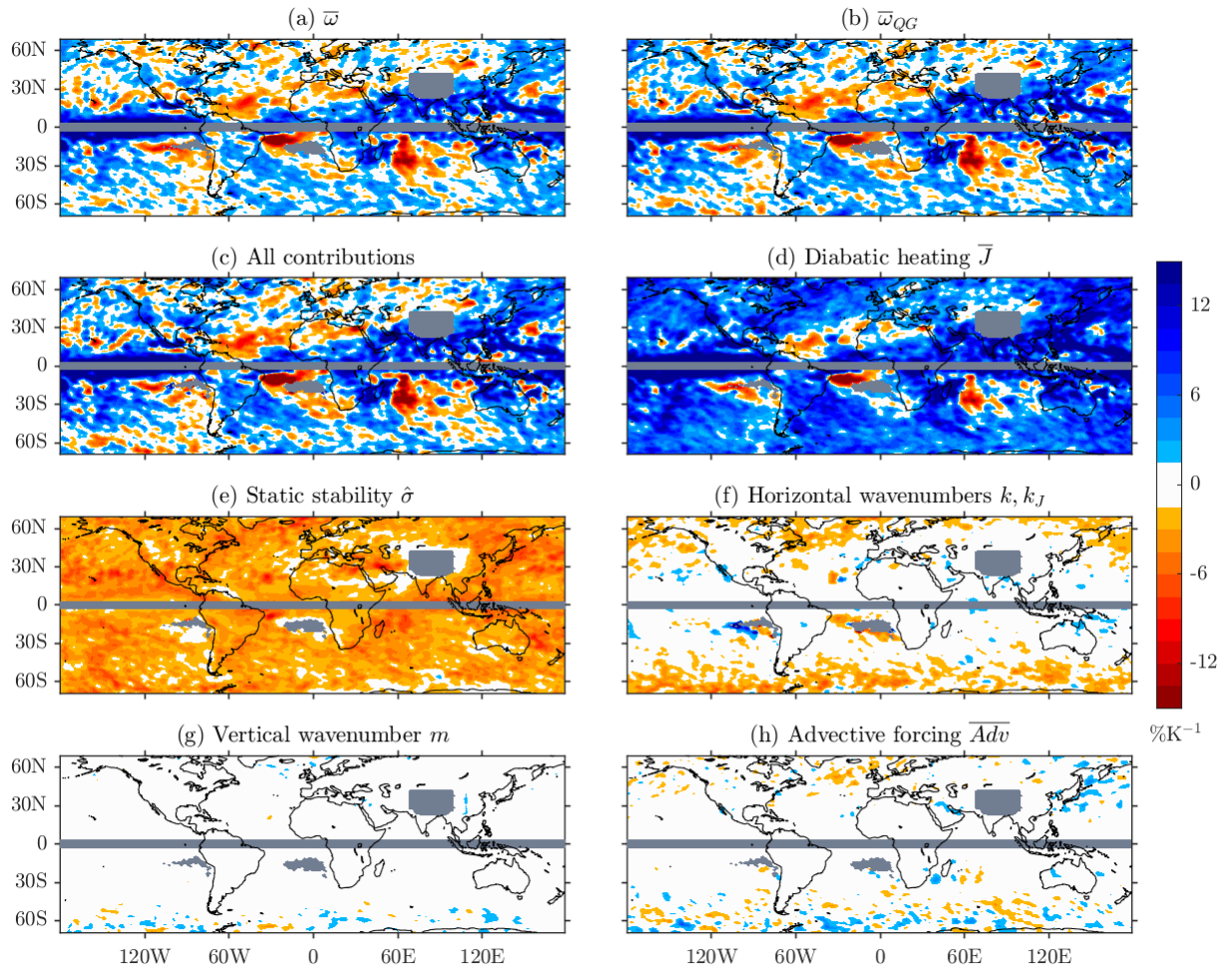


Figure S9. As in Fig. 4, but for daily precipitation extremes in CESM-LE, and grid points with fewer than 5 events are masked.

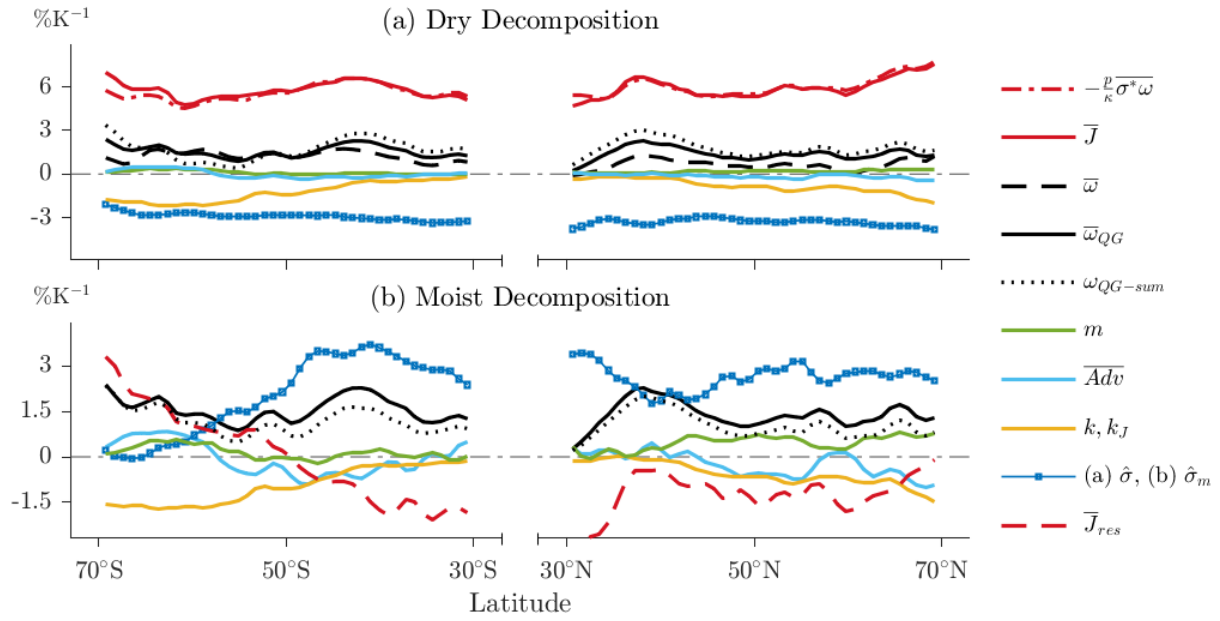


Figure S10. As in Fig. 5, but for daily precipitation extremes in CESM-LE.

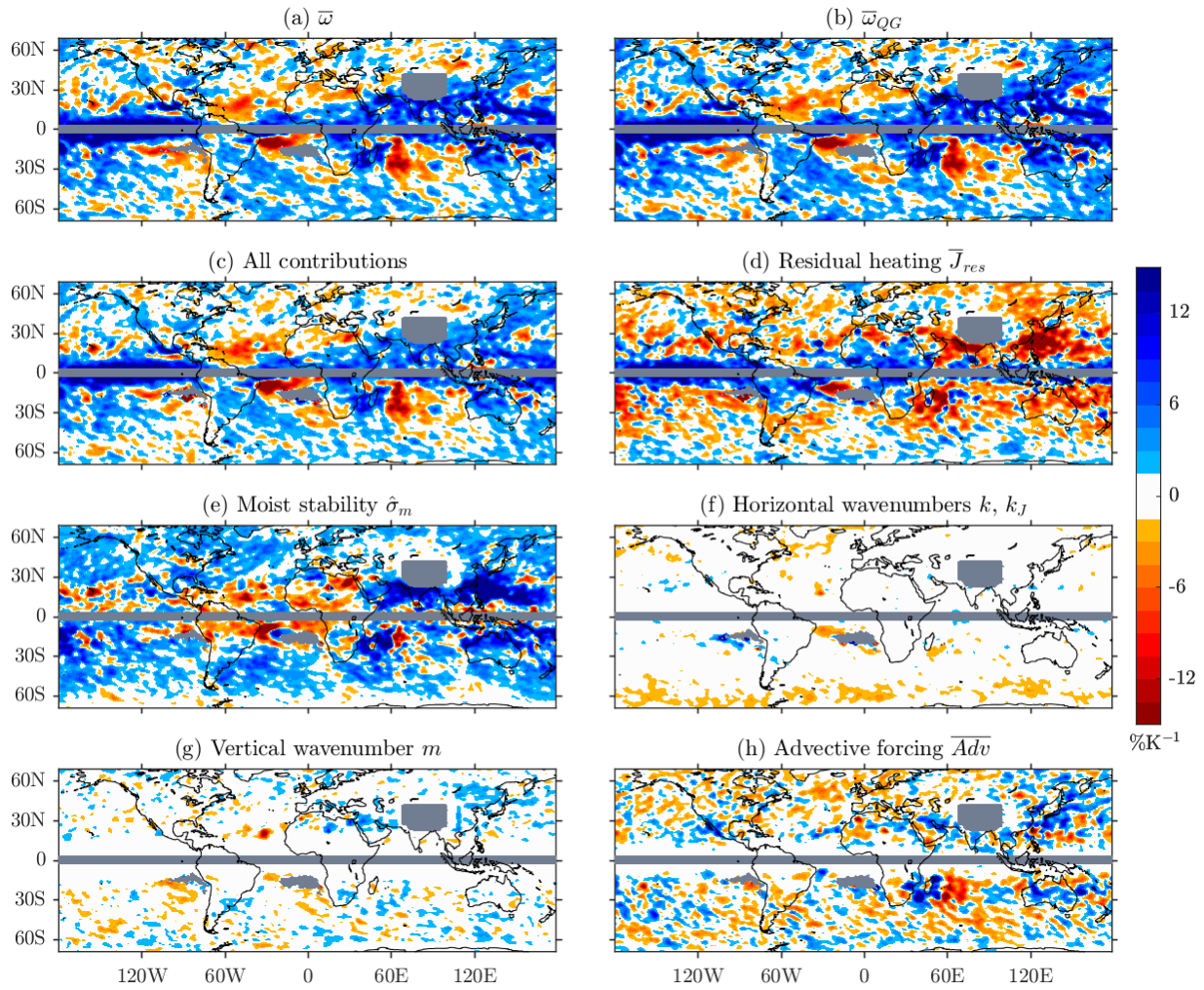


Figure S11. As in Fig. 8, but for daily precipitation extremes in CESM-LE, and grid points with fewer than 5 events are masked.

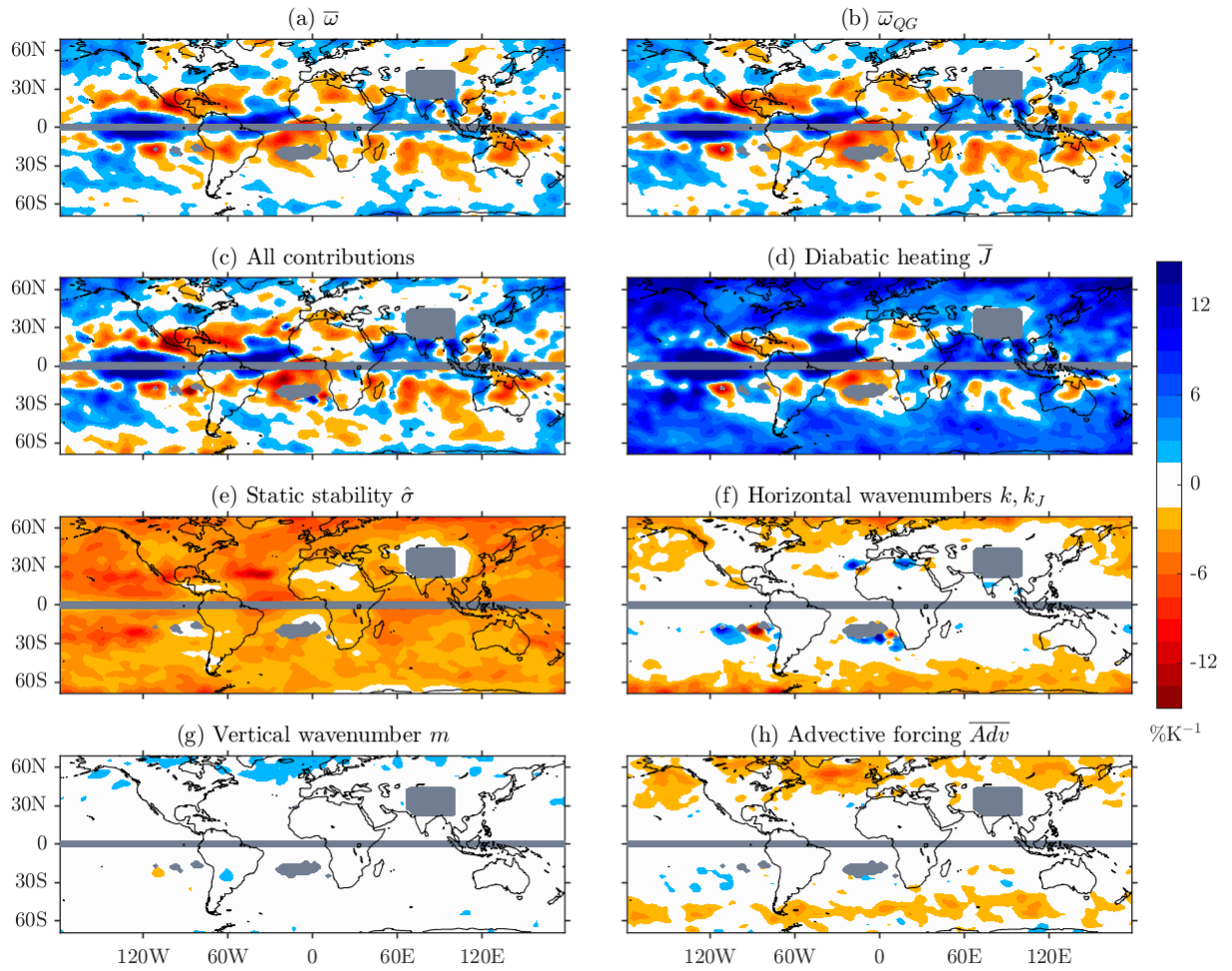


Figure S12. As in Fig. 4, but for daily precipitation extremes at the 99.5-percentile in GFDL-CM3, and grid points with fewer than 5 events are masked.

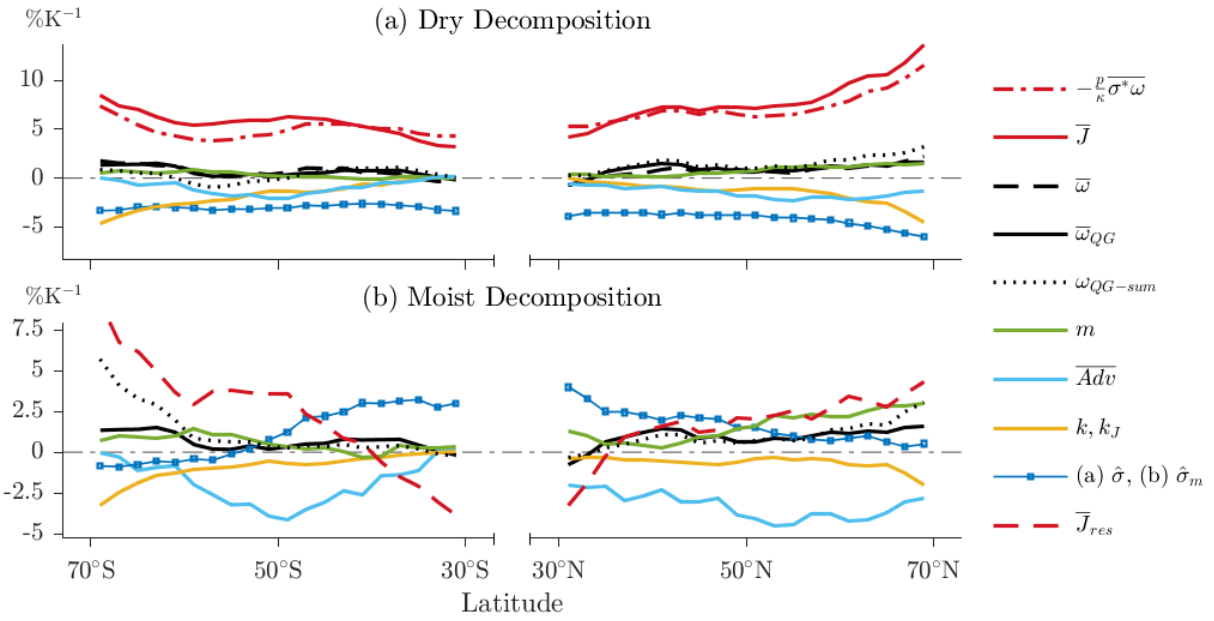


Figure S13. As in Fig. 5, but for daily precipitation extremes at the 99.5-percentile in GFDL-CM3.

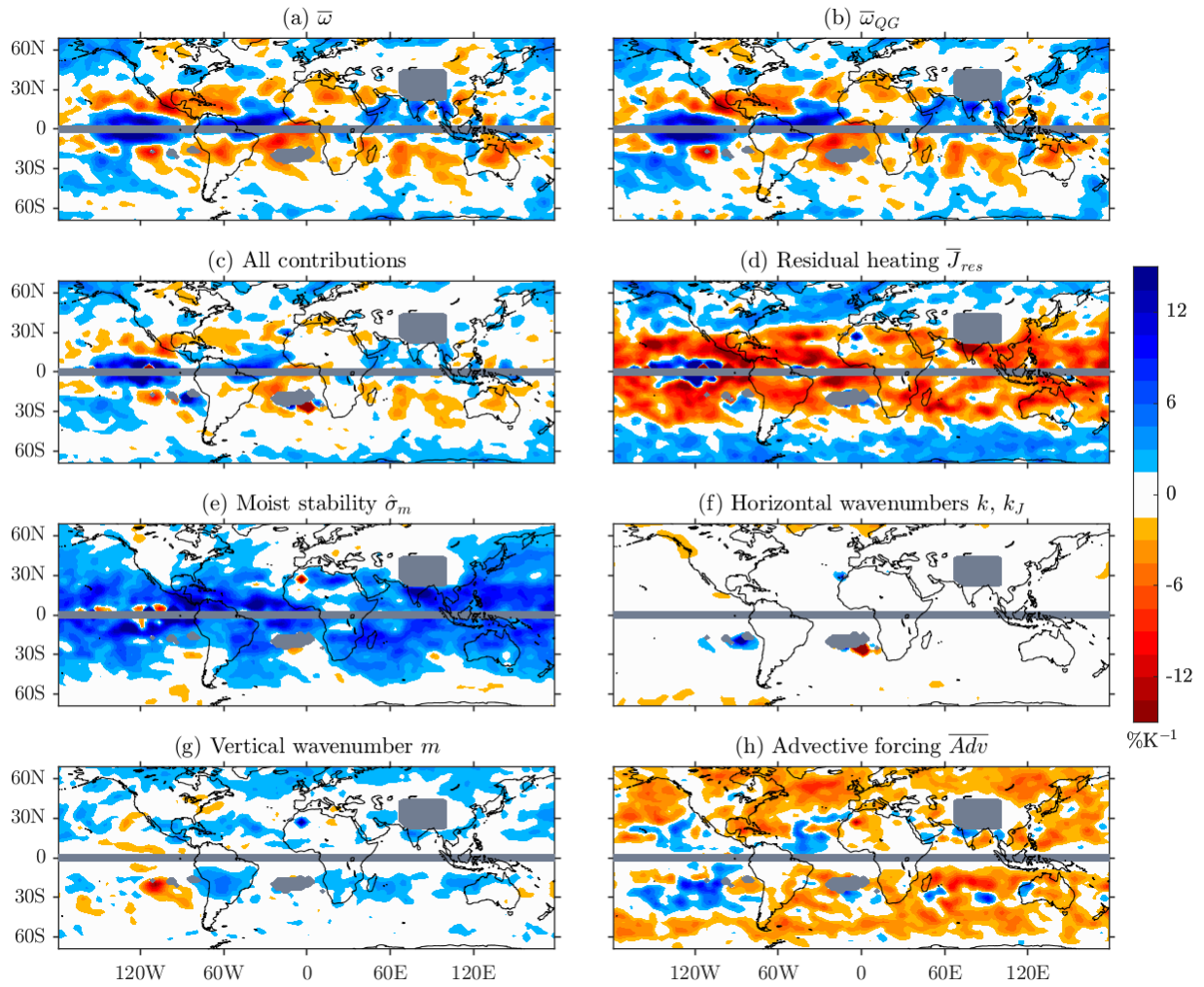


Figure S14. As in Fig. 8, but for daily precipitation extremes at the 99.5-percentile in GFDL-CM3.